Physics and Imaging in Radiation Oncology 16 (2020) 103–108

Contents lists available at ScienceDirect

Physics and Imaging in Radiation Oncology

journal homepage: www.sciencedirect.com/journal/physics-and-imaging-in-radiation-oncology

Original Research Article

Investigation of planar image quality for a novel 2.5 MV diamond target beam from a radiotherapy linear accelerator

Jennifer M. Borsavage [a,*], Amanda Cherpak [a,b,c], James L. Robar [a,b,c]

[a] Dalhousie University, Department of Physics and Atmospheric Science, 5820 University Ave., Halifax, Nova Scotia B3H 1V7, Canada
[b] Dalhousie University, Department of Radiation Oncology, 5820 University Ave., Halifax, Nova Scotia B3H 1V7, Canada
[c] Nova Scotia Health Authority, Department of Medical Physics, Halifax, Canada

ARTICLE INFO

Keywords:
Low-Z target
Beam's eye view imaging
Diamond target
Planar imaging
MV imaging

ABSTRACT

Background and purpose: A commercial 2.5 MV beam has been clinically available for beam's-eye-view imaging in radiotherapy, offering improved contrast-to-noise ratio (CNR) compared to therapeutic beams, due to the softer spectrum. Previous research suggested that imaging performance could be improved using a low-Z diamond target to reduce the self-absorption of diagnostic energy photons. The aim of this study was to 1) investigate the feasibility of two 2.5 MV diamond target beamline configurations and 2) characterize the dosimetry and planar image quality of these novel low-Z beams.

Materials and methods: The commercial 2.5 MV beam was modified by replacing the copper target with sintered diamond. Two beamlines were investigated: a carousel-mounted diamond target beamline and a 'conventional' beamline, with the diamond target in the target arm. Planar image quality was assessed in terms of spatial resolution and CNR.

Results: Due to image artifacts, image quality could not be assessed for the carousel-mounted low-Z target beam. The 'conventional' 2.5 MV low-Z beam quality was softer by 2.7% compared to the commercial imaging beam, resulting in improved CNR by factors of up to 1.3 and 1.7 in thin and thick phantoms, respectively. In regard to spatial resolution, the 'conventional' 2.5 MV low-Z beam slightly outperformed the commercial imaging beam.

Conclusion: With a simple modification to the 2.5 MV commercial beamline, we produced an improved energy spectrum for imaging. This 2.5 MV diamond target beam proved to be an advantageous alternative to the commercial target configuration, offering both superior resolution and CNR.

1. Introduction

High atomic number (Z) targets have proven unfavorable in megavoltage (MV) imaging beamlines due to self-absorption of diagnostic energy photons (i.e. in the range 25–150 keV) [1]. Consequently, MV imaging is associated with poor image contrast characteristics due to the Compton dominant interactions of photons in the MV spectrum. Image quality has been further compromised by the low efficiency of typical MV detectors, which is on the order of 1–2% [2]. Kilovoltage (kV) on-board imaging systems offer substantially better image quality than MV; however, these auxiliary systems introduce increased cost and maintenance, additional uncertainties [3], and prevent visualization of the treatment volume relative to the collimation of the beam during treatment [4].

While the kV system has provided superior image quality, the drawbacks of the system, as well as the potential for improved beam's-eye-view (BEV) image guidance, motivated the continued development of MV beams, such as the introduction of a commercial 2.5 MV FFF beam. With a lower nominal energy, this 2.5 MV beam contains a greater proportion of diagnostic energy photons compared to a 6 MV therapy beam, for example, comprised 22% of photons in the diagnostic range [5] versus less than 1% for 6 MV [6]. This increased proportion of diagnostic energy photons resulted in increased contrast by factors of 2.5 to 3.6 times compared to 6 MV. Previous studies have suggested that this 2.5 MV low-X beam could be improved by replacing the current high-Z copper target with low-Z sintered diamond to further soften the spectrum [5,7]. The softer spectrum of the 2.5 MV low-Z beam should increase the absolute contrast between tissues and the achievable contrast-to-noise ratio (CNR), due to the $(h\nu)^{-3}$ dependence of the photoelectric mass attenuation coefficient [8]. Additionally, the CNR per unit dose should increase due to the increased detection quantum efficiency (DQE) of the diagnostic energy photons in the MV spectrum.

* Corresponding author.
E-mail address: Jennifer.Borsavage@dal.ca (J.M. Borsavage).

https://doi.org/10.1016/j.phro.2020.10.007
Received 29 February 2020; Received in revised form 9 October 2020; Accepted 14 October 2020
Available online 5 November 2020

Parsons *et al.* previously evaluated the commercial 2.5 MV low-X beam against a low-Z 2.35 MV carbon target beam using Monte Carlo simulations in VirtuaLinac [9] and EGSnrc [10]. Compared to the 2.5 MV low-X beam, this group observed an increase in the relative fraction of diagnostic energy photons by 10%, resulting in increased contrast by factors of 1.28 and 1.35 for thin and thick phantoms, respectively [5].

A variety of low-Z targets have been previously implemented on several treatment platforms [1,6,11,12,13], but this study marks the first installation on a modern linac. The aim of this study was twofold: 1) to investigate the feasibility of two 2.5 MV sintered diamond target beamline configurations; and 2) to characterize the dosimetric and image quality characteristics of the novel 2.5 MV low-Z target beams in comparison to the commercial 2.5 MV low-X beam. Due to the photoelectric absorption dependence on Z^3, we hypothesized that replacing the 2.5 MV low-X copper target with low-Z sintered diamond would reduce the self-absorption of diagnostic energy photons, producing a softer beam with improved planar CNR.

2. Material and methods

The low-Z target material used in this work was thermally stable polycrystalline (TSP) sintered diamond, a synthetic diamond selected for its low atomic number ($Z \approx 6$) and high melting point. Two low-Z target beamlines were investigated in this work, including: an external target setup with the diamond target mounted in the carousel of the linac, and a more 'conventional' beamline setup, with the diamond target machined into the target arm. Both targets were installed on a TrueBeam STx (Varian Medical Systems, Palo Alto, CA) C-arm linac.

2.1. Carousel-mounted target beamline

The preliminary beamline involved an external target mounted in the carousel of the linac, modeled after targets previously investigated on the Clinac platform [6,11,12]. The target assembly was manufactured to mimic the shape of a flattening filter, allowing for placement of the target as close to the exit window as possible. The cylindrical sintered diamond target was 3.1 mm thick (77% of the continuous slowing down approximation (CSDA) range of incident 2.5 MeV electrons) and 11 mm in diameter, which was maximized given the physical constraints of the beamline geometry. The design for the target assembly was determined by first optimizing the shape of a nylon mockup in an empty port, ensuring adequate clearance during manual rotation of the carousel. Once machined, the target was installed and a procedure was established for operating the 2.5 MV beam with the target arm retracted and the carousel-mounted target in the beamline.

Unlike experiences with analogous beamlines on previous platforms, image quality could not be assessed for our low-Z carousel-mounted target beam due to the presence of a circular artifact in all images acquired with the MV detector (Fig. 4d). The source of the artifact was investigated by examining the integrity of the sintered diamond target, possible detector saturation, resultant dark current in the EPID from successive acquisition, and the incident electron beam spot size. The beam spot size was measured at various locations in the beamline including: the base of the carousel, the front face of the target, and at 75 cm SSD using sub-MU exposures on radiochromic film.

2.2. 'Conventional' low-Z target beamline

2.2.1. Target arm machining and installation

The TrueBeam target arm was modified to replace the commercial copper target with a disk of TSP sintered diamond (13.44 mm in diameter, 5 mm thick). The thickness of the diamond disk was selected to be 1.1 times the CSDA range [12] of 2.8 MeV electrons; optimized to account for uncertainties in the incident electron energy, eliminate transmission electrons and filter out photons with energy lower than 25 keV that would contribute increased dose to the patient [1]. Prior to machining, the distance between cooling lines in the arm (~1.7 cm) was measured based on an MV image of the target arm to ensure suitability of the target diameter. The copper target was milled out and the diamond disk secured in place by a lip on the underside of the target, and using a mechanical press from the top face to ensure permanent installation (Fig. 1). Prior to installation, the target arm was externally connected to the TrueBeam cooling system to confirm integrity of the cooling lines. All necessary quality assurance measures were carried out before and after installation to verify consistency of clinical beams. For safety reasons, the 2.5 MV beam was removed from clinical service and assigned solely for research.

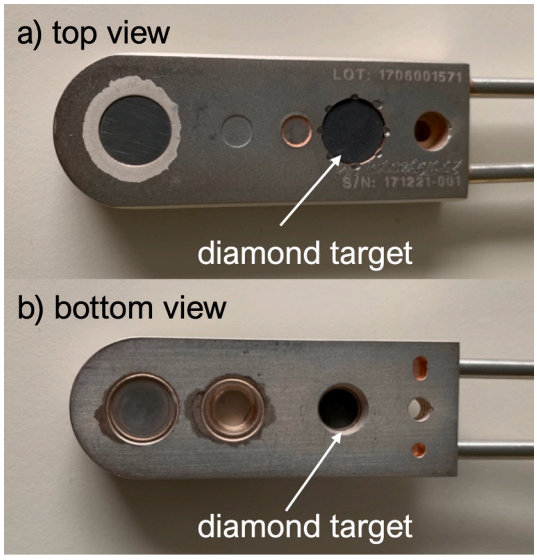

Fig. 1. a) Top view and b) bottom view of experimental TrueBeam target arm showing the sintered diamond target secured into the fourth target position, replacing the low-X copper target.

2.2.2. Planar image quality characterization

Planar image quality was characterized in terms of spatial resolution and CNR. Spatial resolution was evaluated using the relative modulation transfer function (RMTF), following the methodology proposed by Rajapakshe *et al.* [14]. This method utilized the QC3 phantom (Fig. 2a), which contains alternating pairs of high and low-density bars, forming line pair regions of the following spatial frequencies: 0.1, 0.2, 0.25, 0.4 and 0.75 line pairs per mm (lp/mm). For each input square wave frequency in the phantom, the calculated RMTF describes the degree of output signal modulation relative to the lowest spatial frequency. The QC3 phantom was setup to 99 cm SSD, held at a 45° with respect to the axial plane using an acrylic jig to avoid aliasing (Fig. 2b). The phantom was imaged at a gantry angle of 90° with a 14 x 14 cm^2 field using a SID of 150 cm. Multiple images were acquired for each beam to estimate uncertainty in RMTF calculations.

RMTF was calculated using Eq. (1), where $M(f)$ is the modulation of a given spatial frequency, f, and $M(f_1)$ is the modulation of the lowest spatial frequency (i.e. 0.1 lp/mm).

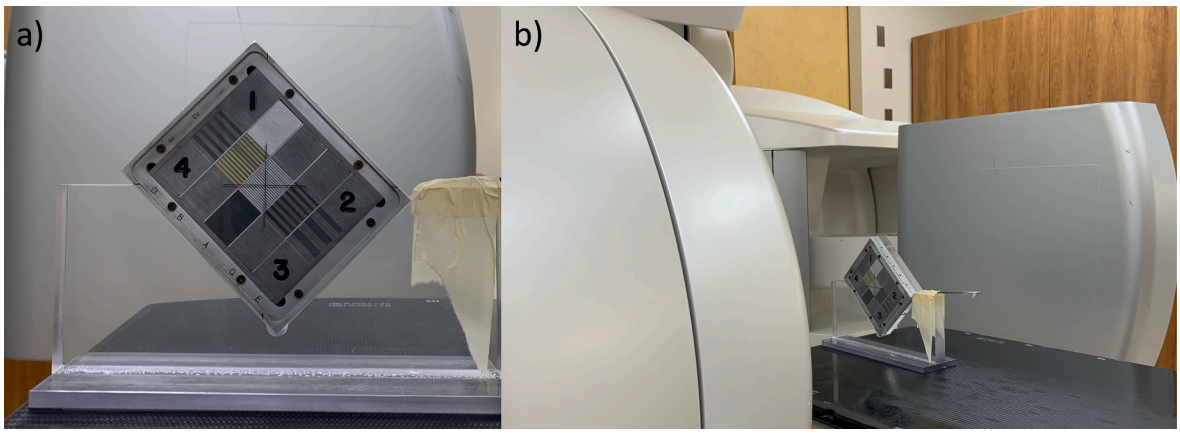

Fig. 2. a) The QC3 phantom containing regions of various frequency bar patterns and b) the QC3 phantom setup at 99 cm SSD, at 45° with respect to the axial plane, for RMTF calculations.

Fig. 3. a) In-house contrast phantom containing 1) CB2-30% 2) breast 3) cortical bone 4) brain tissue equivalent inserts and two voids for additional materials and b) thin contrast phantom imaging setup at 98 cm SSD.

$$RMTF(f) = \frac{M(f)}{M(f_1)} \tag{1}$$

As suggested by Droege and Morin [15], signal modulation was calculated using Eq. (2), where $\sigma_m^2(f)$ is the total variance in a given line pair region and $\sigma^2(f)$ is the variance due to random noise within the same region.

$$M^2(f) = \sigma_m^2(f) - \sigma^2(f) \tag{2}$$

The contributions due to random noise were removed from the signal modulation by subtracting sequential images. Since the variances of the two subtracted images are assumed equal, the variance due to random noise was calculated using Eq. (3), as outlined by Rajapakshe *et al* [14].

$$\sigma^2(f) = \frac{\sigma_{sub}^2(f)}{2} \tag{3}$$

CNR was evaluated using an in-house phantom containing low- to high-contrast tissue equivalent inserts (Gammex, Middleton, WI), including brain, breast, CB2-30%, and cortical bone for thin (4 cm) and thick (20 cm) phantoms (Fig. 3a) [11]. The inserts were arranged in a 14 cm-diameter circle centered on an inscribed crosshair on the top face of the solid water phantom (30 × 30 × 2 cm^3) for alignment with the beam's central axis. Two phantom thicknesses were constructed by wedging the contrast phantom between equivalent thicknesses of solid water to constitute the total phantom thickness (i.e. 4 and 20 cm). The phantoms were setup isocentrically and imaged at a gantry angle of 90° to avoid contributions of couch scatter to acquired images (Fig. 3b).

Images were acquired using a 20 × 20 cm^2 field at a SID of 150 cm with MU values defined to span imaging doses of 0.1 mGy – 5 cGy. Images were acquired using the experimental 2.5 MV low-Z beam, the commercial 2.5 MV low-X beam and 6 MV beam for comparison. For each beam, three images were acquired at each dose to account for fluctuations in output. CNR was evaluated for each tissue equivalent insert using Eq. (4), where *ROI* is a circular region of interest sampled at the center of the insert in the image, *bg* represents an annulus surrounding the insert in the image, *P* is the average pixel intensity and σ^2 represents the variance in the corresponding regions.

$$CNR_{ROI} = \frac{\left|\overline{P}_{ROI} - \overline{P}_{bg}\right|}{\sqrt{\sigma_{ROI}^2 + \sigma_{bg}^2}} \tag{4}$$

2.2.3. Imaging dose calculation

The 2.5 MV low-Z and 2.5 MV low-X beams were calibrated using the American Association of Physicists in Medicine's Task Group 51 formalism [16]. PDD curves were acquired for 10 x 10 cm^2 fields at 100 cm SSD to determine beam quality. In a previous study investigating 2.5 MV low-X imaging dose, Ding and Munro [17] calibrated the 2.5 MV low-X output using $k_Q = 1.00$. Assuming negligible differences between the chamber perturbation factors of the 2.5 MV beam and Co-60, they calculated k_Q as the ratio of Spencer-Attix water-to-air stopping-power ratios (SPR) for the two beam energies. The study reported less than 0.1% difference between

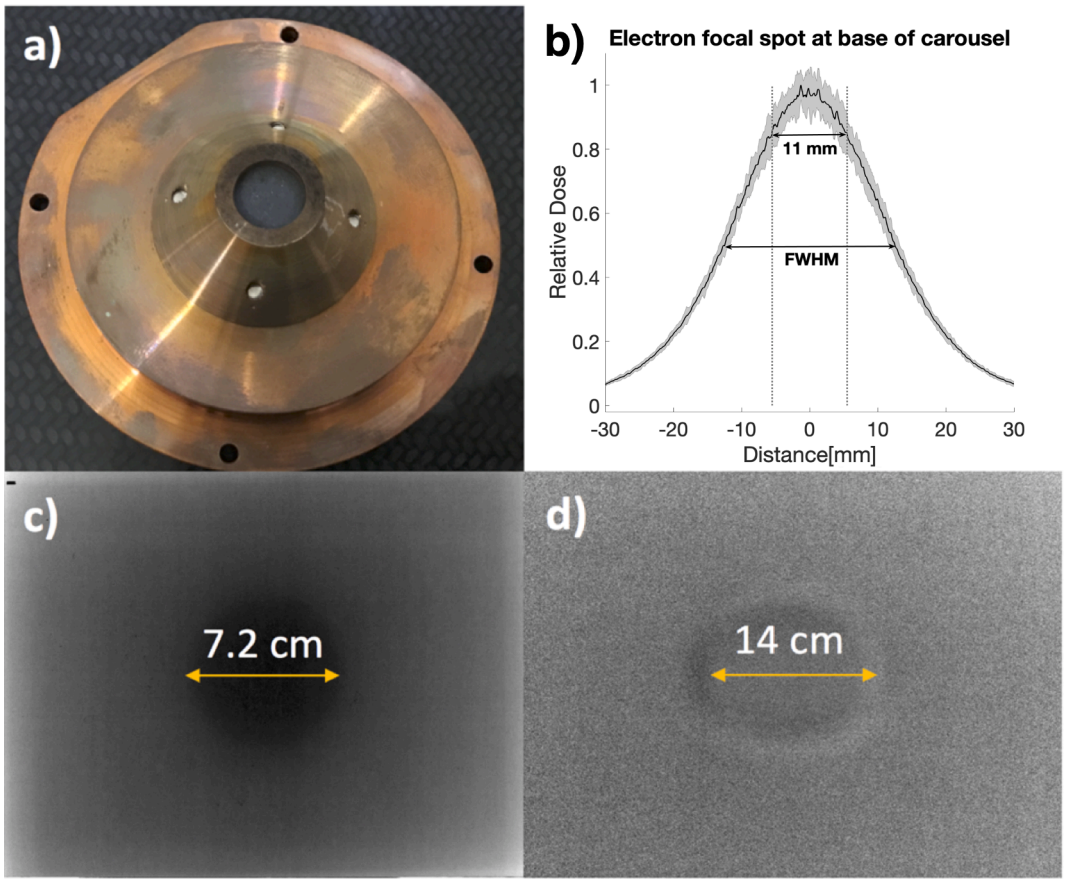

Fig. 4. Pictorial representation of circular artifact investigation showing the a) intact carousel mounted target assembly b) electron focal spot measured with radiochromic film below the target plane showing the diameter of the exposed sintered diamond target (11 mm) and the corresponding FWHM c) radiochromic film image acquired with 2.5 MV diamond target beam at 75 cm SSD and d) EPID acquired test image with 2.5 MV diamond target beam at 150 cm SID.

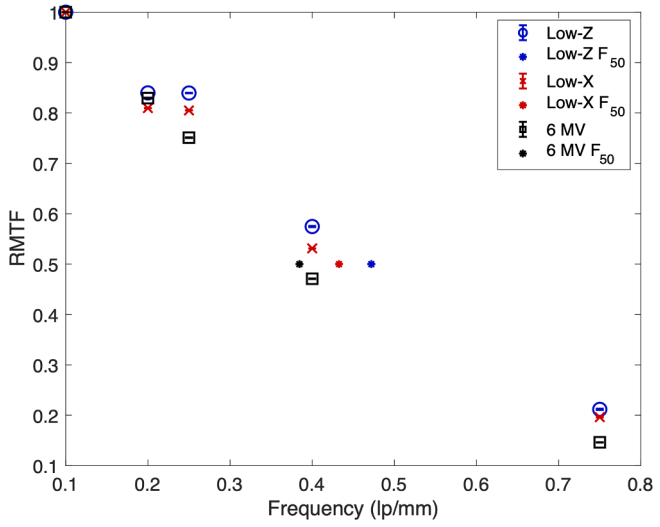

Fig. 5. Relative modulation transfer function of 2.5 MV low-Z, 2.5 MV low-X and 6 MV beams.

the SPR of the 2.5 MV low-X beam and Co-60 at the recommended calibration depth of 10 cm [17], thus concluding $k_Q = 1.00$. Based on Ding and Munro's study [17], and the fact that our measurements found similar beam qualities for the 2.5 MV low-X and 2.5 MV low-Z beams (i.e. 52.85% and 50.15%, respectively), $k_Q = 1.00$ was assumed for both beams.

Dose per MU was calculated for the 2.5 MV low-X and 2.5 MV low-Z beams under reference conditions using an isocentric setup (i.e. 10 × 10 cm^2 field, 90 cm SSD, 10 cm depth). Point dose measurements were performed in water using a calibrated Exradin A12 (Standard Imaging, Middleton WI) ion chamber. Output factors and corresponding TPR measurements were made for a 20 × 20 cm^2 field for both 2.5 MV low-X and 2.5 MV low-Z beams to calculate imaging dose for thin and thick phantom setups. Imaging doses for the 6 MV beam were calculated by modeling the thin and thick solid water phantoms in the treatment planning system (Eclipse version 13.6, Varian, Palo Alto, CA).

3. Results

3.1. Carousel-mounted target beamline

Removal of the carousel-mounted target confirmed that the target was intact (Fig. 4a). Film irradiated at 75 cm SSD verified that the circular artifact was due to the incident electron beam and unrelated to the EPID (Fig. 4c). The film irradiated at the base of the carousel revealed that the full-width-half-maximum (FWHM) of the spot size was 23.5 mm; more than twice the diameter of the diamond target (Fig. 4b). The dose on the periphery of the film irradiated at the level of the target was 58% of that on the central axis; which confirmed that the electron beam spot size was larger than the target. This was deemed an insurmountable limitation of this approach to introducing a diamond target, given that the physical constraints of the installation limited further increase of the target diameter. Furthermore, it would have been physically impossible to have moved the target closer to the exit of the electron beam from the vacuum, where the electron beam might have been sufficiently narrow to create a useful focal spot for imaging.

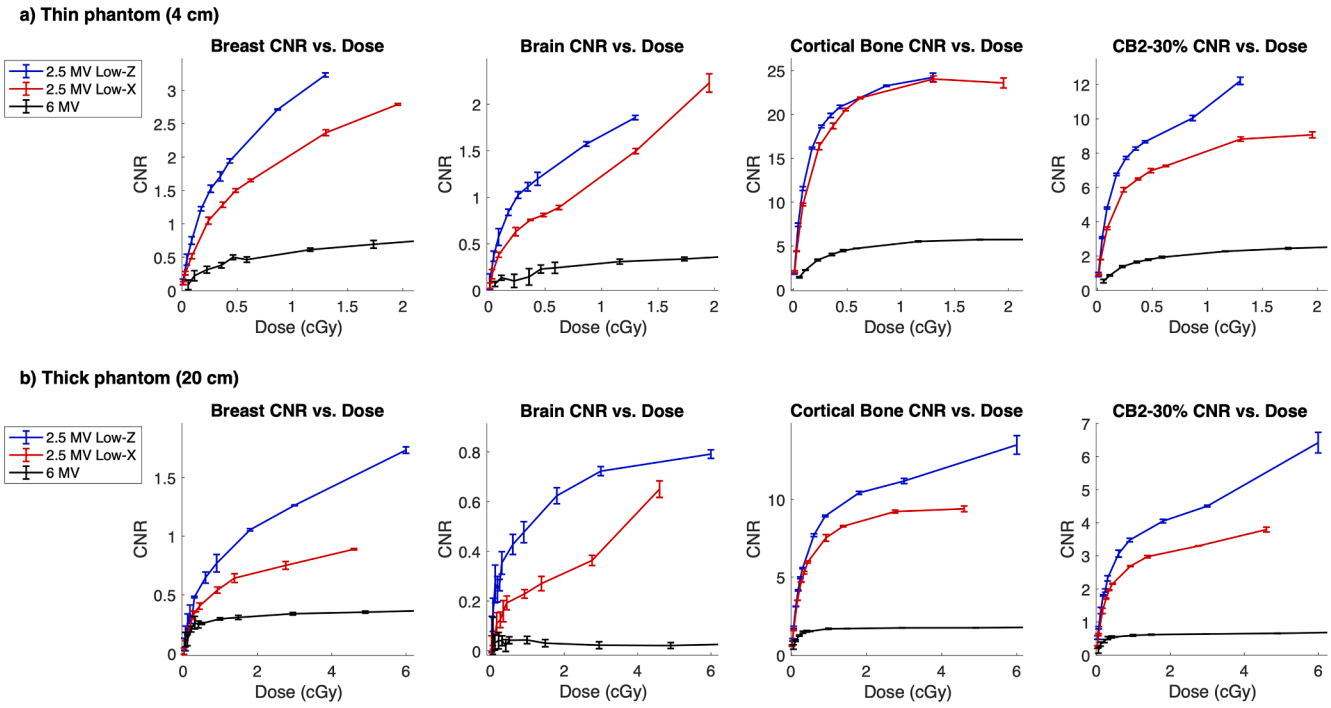

Fig. 6. CNR versus dose for breast, brain, cortical bone, and CB2-30% tissue equivalent inserts in a) thin (4 cm) and b) thick (20 cm) phantoms.

3.2. 'Conventional' low-Z target beamline

3.2.1. Planar image quality characterization

The calculated RMTF, derived from images of the QC3 phantom, showed that our experimental 2.5 MV low-Z beam outperformed the commercial 2.5 MV low-X and 6 MV beams in terms of spatial resolution (see Fig. 5). We observed increases in F_{50}, the frequency at which the RMTF decreases to 50%, by 22.7% and 12.5% for the 2.5 MV low-Z and 2.5 MV low-X beams, compared to 6 MV. This translated to an increase of approximately 0.5 lp/mm, and 1 lp/mm for the 2.5 MV low-Z beam compared to the 2.5 MV low-X and 6 MV beams, respectively. The improved spatial resolution was likely due to reduced extra-focal radiation resulting from the absence of a flattening filter in the 2.5 MV beamlines.

The CNR versus dose results presented in Fig. 6 demonstrated a clear advantage for the 2.5 MV low-Z beam at imaging doses above 1 mGy in the thin phantom and above 3 mGy in the thick phantom, compared to the 2.5 MV low-X beam. At doses above 3 mGy, the CNR of each material in the thick phantom was greater for the low-Z beam than the low-X beam, by factors of 1.4–1.7 for breast, and 1.1–1.3 for cortical bone. The same trend was observed for materials in the thin phantom above 1 mGy, excluding cortical bone. Increases in CNR were observed in breast and CB2-30% in the thin phantom by factors of 1.2–1.3 and 1.2–1.4, respectively. Unlike the other materials in the thin phantom, the difference in the CNR of cortical bone between the low-Z and low-X beams was negligible across all doses. At doses less than 1 mGy, the difference in CNR between images acquired with low-Z and low-X beams were negligible for breast and cortical bone in the thick phantom.

4. Discussion

This work marks the first implementation of a low-Z diamond target beam for 2.5 MV imaging on a modern linac platform. In our investigation, we implemented two beamline geometries including (i) a carousel-mounted target design, and (ii) a 'conventional' setup with the target in the target arm.

Based on our thorough investigation of the carousel-mounted target beamline, we have concluded that the large electron spot size impinges on the copper housing of the target assembly, causing a non-uniform photon fluence below and the appearance of a circular artifact in images acquired by either film or the EPID. This is caused by the geometry of the carousel relative to the exit window, such that the electron scatter in air produces a large focal spot incident on the upstream surface of the target. While the carousel-mounted target design has been used successfully on a previous platform [6,11,12], the redesign of the beamline in the current platform precludes this carousel-mounted target design.

On the other hand, a viable approach is installation of a diamond target in the target arm (our 'conventional' setup), and for this configuration we have evaluated planar image quality compared to the commercial 2.5 MV low-X beam. As hypothesized, replacing the high-Z copper target with low-Z sintered diamond in the 2.5 MV beamline produced a softer beam, as demonstrated by the 2.7% reduction in PDD (10 cm) for the 2.5 MV low-Z beam compared to 2.5 MV low-X. We found similar beam quality to the 2.35 MV carbon target beam modelled by Parsons *et al.* [5], although our 2.5 MV low-Z PDD(10 cm) was greater by 1.6%. This is likely due to the small difference in nominal energy as well as the presence of high-Z sintering materials in our target. Compared to the commercial 2.5 MV low-X beam, the softer low-Z spectrum resulted in improved CNR by factors of up to 1.7, at clinically relevant MV imaging doses. This permits either improved CNR for the same dose, or conversely, decreased imaging dose for the same CNR. We observed advantages of the low-Z beam over the commercial 2.5 MV low-X beam for both thin and thick phantoms, except for cortical bone in the thin phantom and in cases where CNR itself is very low (<1) for all beams, i.e., where the objects were essentially indistinguishable from background.

While this study has focused solely on planar imaging with the low-Z beam, in concept the same beam could be used for cone-beam CT acquisition, and even volume-of-interest CBCT using the MLC for collimation according to the relevant anatomy for the given image guidance task [18]. Although kV imaging provides superior image quality to MV per unit imaging dose, image guidance from the BEV is valuable in the delivery of precision radiation therapy. With a simple modification to the 2.5 MV low-X beamline, we produced a softer energy spectrum for imaging, which improves BEV imaging with better spatial resolution and CNR. We anticipate that additional modifications to the low-Z beamline

could further improve the CNR versus dose characteristics of 2.5 MV BEV imaging. One such alteration, to be examined in forthcoming work, is the removal of the 0.81 mm brass cover-plate from the carousel of the 'conventional' 2.5 MV low-Z target beamline, to further reduce the self-absorption of diagnostic energy photons within the treatment head. Another feasible approach involves modifying the EPID to increase the DQE, such as the integration of a thick CsI flat-panel detector [19].

This study concludes our initial characterization of this novel 2.5 MV diamond target beam for BEV imaging. We demonstrated the ease of installation of a low-Z sintered diamond target beam on a modern linac, and the consequent improvements in CNR as a function of dose compared to the current low-X mode. We suggest sintered diamond as a favorable alternative to the current copper target in the 2.5 MV low-X beamline.

Declaration of Competing Interest

The authors declare the following financial interests/personal relationships which may be considered as potential competing interests: The authors received research support from Varian Medical Systems.

Acknowledgements

The authors would like to thank Varian Medical Systems for financial support through a research collaboration. Additional acknowledgement is extended to David Parsons for his carousel-mounted target design and continued support, Ian Conrod for fabrication of the target arm and contrast phantom, Scott Purcell for installation of the modified target arm, and Robert Moran for continued electronic and technical support.

References

[1] Ostapiak OZ, O'Brien PF, Faddegon BA. Megavoltage imaging with low-Z targets: implementation and characterization of an investigational system. Med Phys 1998; 25:1910–8.
[2] Rottmann J, Morf D, Fueglistaller R, Zentai G, Star-Lack J, Berbeco R. A novel EPID design for enhanced contrast and detective quantum efficiency. Phys Med Biol 2016;61:6297–306. https://doi.org/10.1088/0031-9155/61/17/6297.
[3] Groh BA, Siewerdsen JH, Drake DG, Wong JW, Jaffray DA. A performance comparison of flat-panel imager-based MV and kV cone-beam CT. Med Phys 2002; 29:967–75. https://doi.org/10.1118/1.1477234.
[4] Robar JL. Beam's eye view imaging with low atomic number linear accelerator targets. In: Berbeco R, editor. Beam's eye view imaging in radiation oncology. Boca Raton: Taylor & Francis; 2018. p. 139–62.
[5] Parsons D, Robar JL, Sawkey D. A Monte Carlo investigation of low-Z target image quality generated in a linear accelerator using Varian's VirtuaLinac. Med Phys 2014;2:021719. https://doi.org/10.1118/1.4861818.
[6] Orton EJ, Robar JL. Megavoltage image contrast with low-atomic number target materials and amorphous silicon electronic portal imagers. Phys in Med and Biol 2009;54:1275–89. https://doi.org/10.1088/0031-9155/54/5/012.
[7] Sawkey D, Lu M, Morin O, Aubin M, Gottschalk AR, Bani-Hashemi A, et al. A diamond target for megavoltage cone-beam CT. Med Phys 2010;37:1246–53. https://doi.org/10.1118/1.3302831.
[8] Khan FM, Gibbons JP. Khan's The physics of radiation therapy. 5th ed. Philadelphia: Lippincott Williams & Wilkins; 2014.
[9] Sawkey D. VirtuaLinac Documentation 1.3.0. 2017.
[10] Kawrakow I. Accurate condensed history Monte Carlo simulation of electron transport. I. EGSnrc, the new EGS4 version. Med Phys 2000;27:485–98.
[11] Parsons D, Robar JL. Beam generation and planar imaging at energies below 2.40 MeV with carbon and aluminum linear accelerator targets. Med Phys 2012;39: 4568–78. https://doi.org/10.1118/1.4730503.
[12] Connell T, Robar JL. Low-Z target optimization for spatial resolution improvement in megavoltage imaging. Med Phys 2010;37:124–31. https://doi.org/10.1118/1.3267040.
[13] Faddegon BA, Wu V, Pouliot J, Gangadharan B, Bani-Hashemi A. Low dose megavoltage cone beam computed tomography with an unflattened 4 MV beam from a carbon target. Med Phys 2008;35:5777–86. https://doi.org/10.1118/1.3013571.
[14] Rajapakshe R, Luchka K, Shalev S. A quality control test for electronic portal imaging devices. Med Phys 1996;23:1237–44.
[15] Droege RT, Morin RL. A practical method to measure the MTF of CT scanners. Med Phys 1982;9:758–60.
[16] Almond PR, Biggs PJ, Coursey BM, Hanson WF, Saiful Huq M, Nath R, et al. AAPM's TG-51 protocol for clinical reference dosimetry of high-energy photon and electron beams. Med Phys 1999;26:1847–70.
[17] Ding GX, Munro P. Characteristics of 2.5 MV beam and imaging dose to patients. Radiother and Oncol 2017;125:541–7. https://doi.org/10.1016/j.radonc.2017.09.023.
[18] Leary D, Robar JL. CBCT with specification of imaging dose and CNR by anatomical volume of interest. Med Phys 2014;41. https://doi.org/10.1118/1.4855835. 011909.
[19] Tang G, Moussot C, Morf D, Seppi E, Amols H. Low-dose 2.5 MV cone-beam computed tomography with thick CsI flat-panel imager. J Appl Clin Med Phys 2016;17:235–45. https://doi.org/10.1120/jacmp.v17i4.6185.